RadioGraphics

TEACHING POINTS
See last page

Interactive Web-based Learning Module on CT of the Temporal Bone: Anatomy and Pathology[1]

Grace S. Phillips, MD • Sung E. LoGerfo, MD • Michael L. Richardson, MD • Yoshimi Anzai, MD

An interactive Web-based learning module on the temporal bone has been developed. It shows normal temporal bone anatomy in four imaging planes: axial, coronal, and parallel and perpendicular to the long axis of the petrous bone. After reviewing the normal anatomy, users should be able to identify key imaging features of pathologic conditions of the temporal bone. Children with congenital abnormalities of the temporal bone may present with conductive or sensorineural hearing loss or both and may have a genetic syndrome. Acute otitis media is the most common infection of the temporal bone and is most prevalent among children. Although imaging is unnecessary in uncomplicated otitis media, it is important for evaluation of infectious complications. Classically, temporal bone fractures were described as longitudinal or transverse with respect to the long axis of the petrous bone. However, it is increasingly recognized that many fractures have both longitudinal and transverse components. Patients with temporal bone fractures may have conductive or sensorineural hearing loss in addition to other complications. The most common tumor of the temporal bone at the cerebellopontine angle is the vestibular schwannoma. Paraganglioma is the second most common tumor of the temporal bone and the most common tumor of the middle ear. Supplemental material available at *http://uwmsk.org/temporalbone/atlas.html*

EDITOR'S NOTE

Content of the online supplemental material linked to this article was made available only for educational purposes by the authors, who are solely responsible for all materials contained therein and which are not copyrighted by the RSNA. None of the online supplemental material can be downloaded by readers for any purpose.

ONLINE-ONLY CME

This journal-based CME activity has been approved for ***AMA PRA Category 1 Credit™****. See www.rsna.org/education/rg_cme.html*

LEARNING OBJECTIVES

After completing this journal-based CME activity, participants will be able to:

- Discuss some of the more common congenital anomalies of the ear.
- Describe the role of imaging in evaluation of temporal bone infections and trauma.
- List the key imaging features of tumors and tumorlike conditions of the temporal bone.

Abbreviations: AOM = acute otitis media; CHARGE = coloboma of the eye, heart anomaly, choanal atresia, retardation, genital and ear anomalies; EAC = external auditory canal; ELST = endolymphatic sac tumor; IAC = internal auditory canal; ICA = internal carotid artery; SNHL = sensorineural hearing loss

RadioGraphics 2012; 32:E85–E105 • **Published online** 10.1148/rg.323115117 • **Content Codes:** CT HN NR

[1]From the Department of Radiology, University of Washington School of Medicine, Box 357115, 1959 NE Pacific St, Seattle, WA 98195. Recipient of a Cum Laude award for an education exhibit at the 2010 RSNA Annual Meeting. Received May 13, 2011; revision requested August 24 and received October 11; accepted November 2. For this journal-based CME activity, the authors, editor, and reviewers have no relevant relationships to disclose. **Address correspondence to** G.S.P. (e-mail: *grace.phillips@seattlechildrens.org*).

See also the article by Joshi et al (pp 683-698) in this issue.

Introduction

The anatomy of the temporal bone is complex and is further complicated by the small size and three-dimensional orientation of associated structures. Computed tomography (CT) has revolutionized imaging of the temporal bone. Recent advances in multisection CT scanners allow acquisition of high-resolution volumetric data that enable image reformation in any plane.

Despite the small relative size of the temporal bone, a wide array of pathologic conditions may affect it. Furthermore, there is overlap of the clinical symptoms of pathologic entities arising from the temporal bone. Thus, the combination of a detailed clinical history in conjunction with examination by means of dedicated temporal bone CT facilitates diagnosis of these diseases.

An interactive Web-based learning module on the temporal bone has been developed (*http://uwmsk.org/temporalbone/atlas.html*) that provides the user with an opportunity to review normal temporal bone anatomy. In this article, we present the pertinent normal anatomy in the four standard planes, along with abnormal cases involving four broad categories of disease affecting the temporal bone: congenital malformations, inflammatory conditions, trauma, and tumors and tumorlike conditions. The learning module also includes a self-assessment quiz with questions pertaining to these four general categories.

Embryology

The embryologic development of the ear is a multistage and anatomically complex process. The outer ear structures develop from the first branchial cleft and the first and second branchial arches during the 6th through 12th weeks of intrauterine life (1). The external auditory canal (EAC) initially develops as a solid core of epithelium, termed the *meatal plate*, which migrates toward the first pharyngeal pouch and subsequently hollows out during the 2nd through 7th months of intrauterine life (1). The eustachian tube and tympanic cavity arise from the first pharyngeal pouch between 10 and 30 weeks gestation (1). The tympanic membrane is derived from three germ cell layers, including ectoderm from the first branchial groove and mesoderm and endoderm from the first branchial pouch (1). The ossicular chain and supporting ligaments arise from the first and second branchial arches.

The membranous portion of the inner ear arises from neuroectoderm (otic placode) in the 4th week of gestation. The otic placode invaginates, forming the otic pit, and subsequently forms the otic vesicle (otocyst) (1). The otocyst divides into the dorsal and ventral pouches (pars superior and inferior, respectively), which are the precursors to the utricle, semicircular canals, cochlear duct, and saccule. The bony labyrinth (otic capsule) develops from mesenchyme around the membranous labyrinth between 4 and 8 weeks gestation, continues to grow between 8 and 16 weeks gestation, and ossifies by the 24th week of gestation (1).

Technique

Axial CT images are acquired through the temporal bones. At our institution, 0.625-mm axial sections are then reprocessed and reformatted into magnified axial and coronal images and displayed at 0.3-mm intervals with overlap. In addition to the traditional axial and coronal views (Figs 1, 2), it has become routine at our institution to also perform reformation in the Stenvers

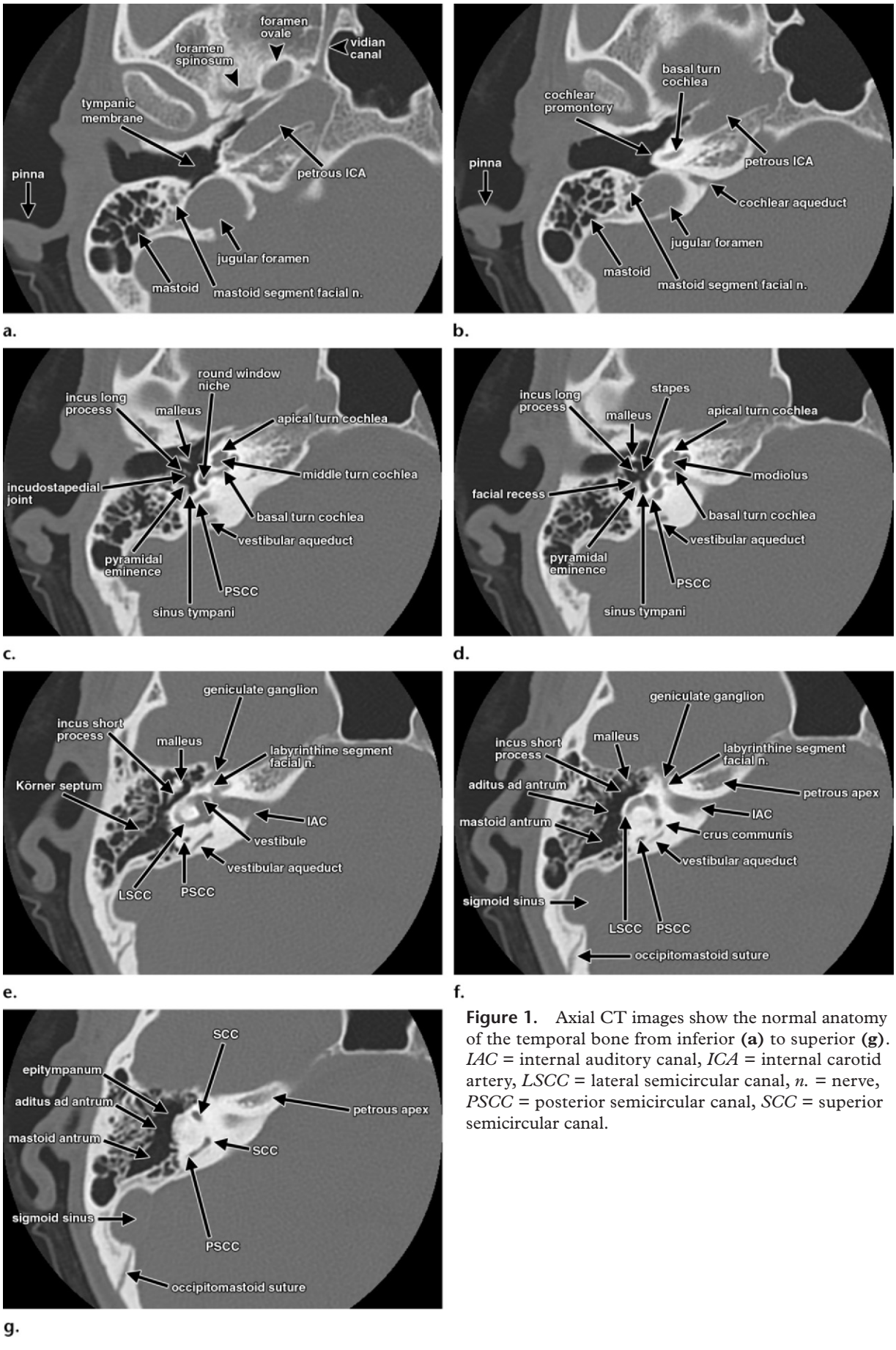

Figure 1. Axial CT images show the normal anatomy of the temporal bone from inferior **(a)** to superior **(g)**. *IAC* = internal auditory canal, *ICA* = internal carotid artery, *LSCC* = lateral semicircular canal, *n.* = nerve, *PSCC* = posterior semicircular canal, *SCC* = superior semicircular canal.

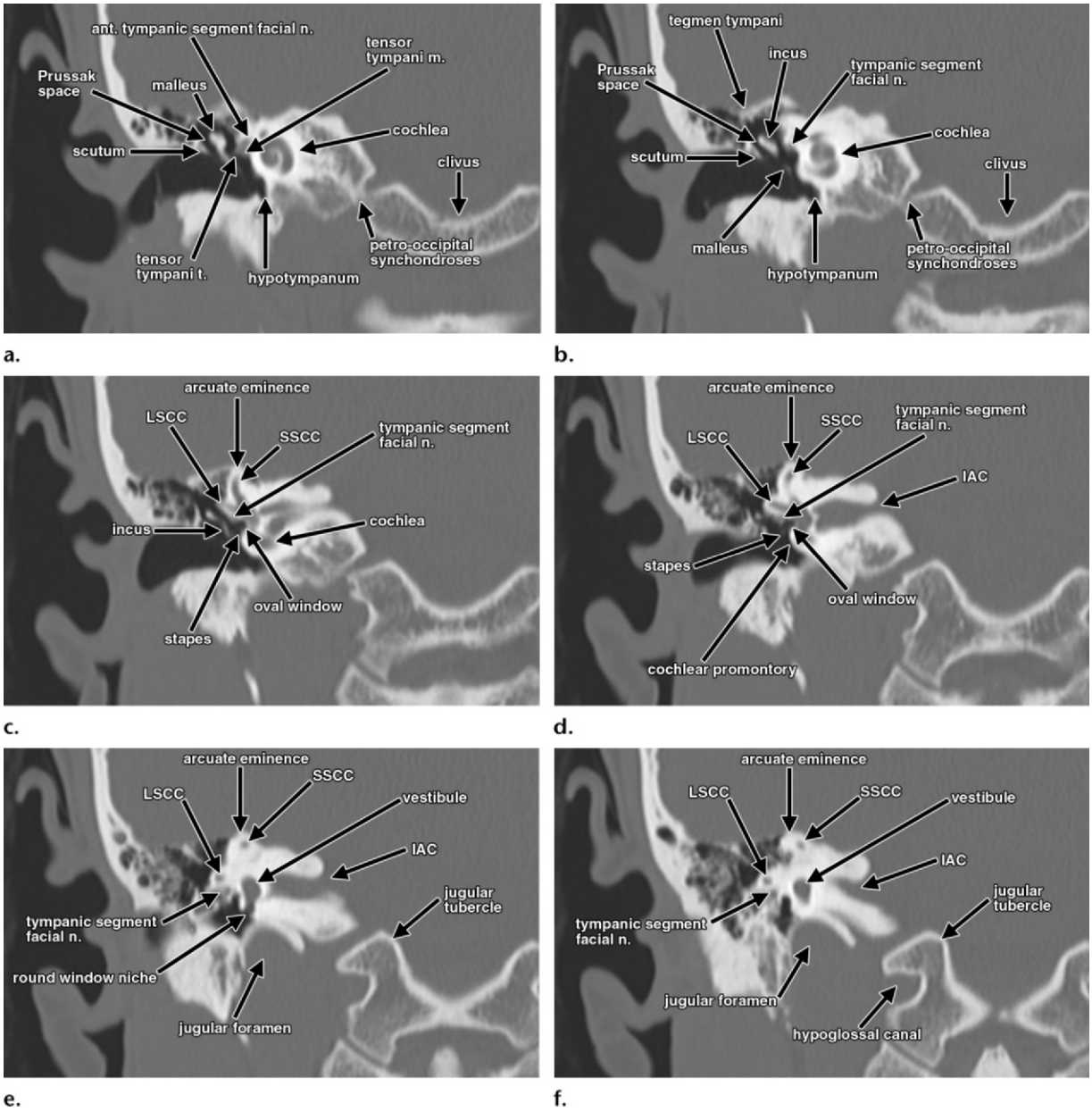

Figure 2. Coronal CT images show the normal anatomy of the temporal bone from anterior **(a)** to posterior **(f)**. *ant.* = anterior, *LSCC* = lateral semicircular canal, *m.* = muscle, *n.* = nerve, *SSCC* = superior semicircular canal, *t.* = tendon.

and Pöschl projections (Figs 3, 4). The Stenvers projection is the plane parallel to the long axis of the petrous bone, and the Pöschl projection is the plane perpendicular to the long axis of the petrous bone. These additional planes are useful for evaluating the structures of the middle and inner ear, which may not be as well seen in the standard axial and coronal planes (2). Magnetic resonance (MR) imaging may be used to evaluate the eighth cranial nerve, which is typically best seen on heavily T2-weighted images in the axial and oblique projections.

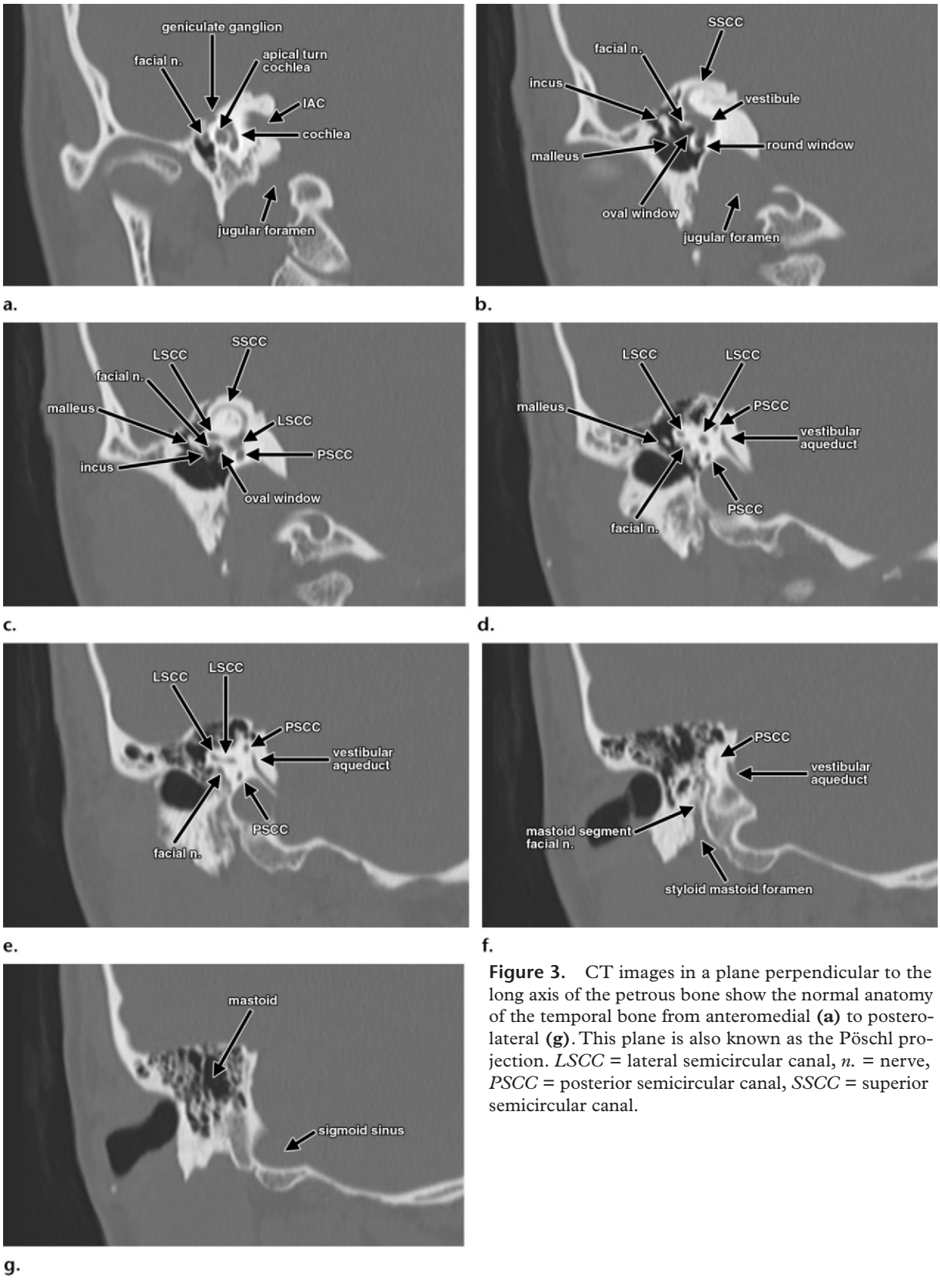

Figure 3. CT images in a plane perpendicular to the long axis of the petrous bone show the normal anatomy of the temporal bone from anteromedial **(a)** to posterolateral **(g)**. This plane is also known as the Pöschl projection. *LSCC* = lateral semicircular canal, *n.* = nerve, *PSCC* = posterior semicircular canal, *SSCC* = superior semicircular canal.

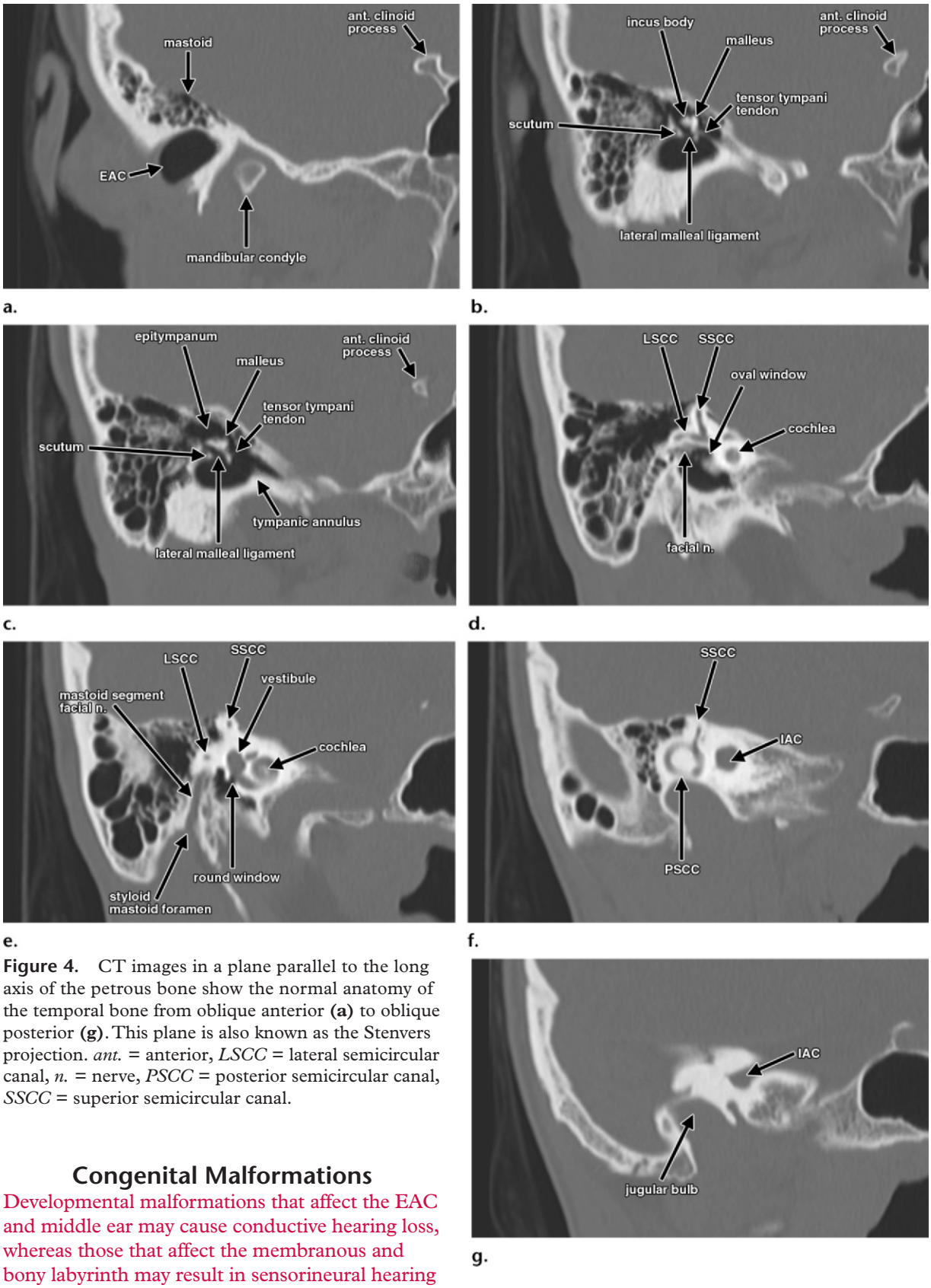

Figure 4. CT images in a plane parallel to the long axis of the petrous bone show the normal anatomy of the temporal bone from oblique anterior **(a)** to oblique posterior **(g)**. This plane is also known as the Stenvers projection. *ant.* = anterior, *LSCC* = lateral semicircular canal, *n.* = nerve, *PSCC* = posterior semicircular canal, *SSCC* = superior semicircular canal.

Congenital Malformations

Teaching Point

Developmental malformations that affect the EAC and middle ear may cause conductive hearing loss, whereas those that affect the membranous and bony labyrinth may result in sensorineural hearing loss (SNHL). Furthermore, congenital hearing deficits can be nongenetic or genetic in origin. Congenital hearing deficits from genetic causes may occur in isolation or in association with various syndromes, such as the CHARGE (coloboma of the eye, heart anomaly, choanal atresia, retardation, genital and ear anomalies), Klippel-Feil,

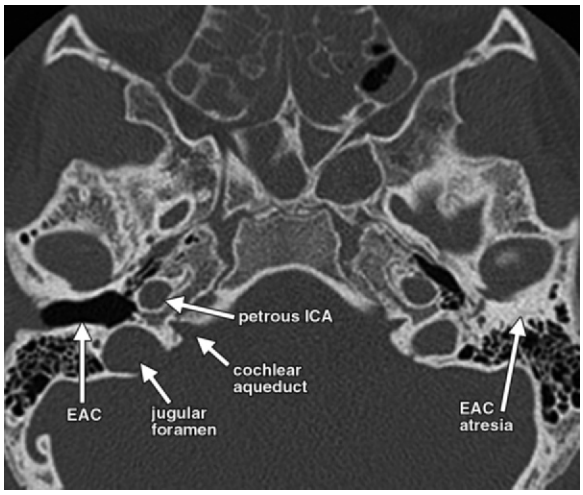

Figure 5. Atresia of the EAC in a 12-year-old boy with left conductive hearing loss and left microtia. Axial CT image shows absence of the left EAC. The left middle ear cavity is small. The right EAC is normal.

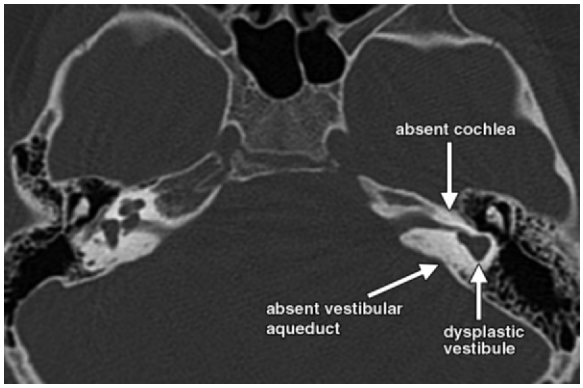

Figure 6. Cochlear aplasia in a 4-year-old girl with profound left SNHL. Axial CT image shows absence of the left cochlea and vestibular aqueduct. The left vestibule and lateral semicircular canal are dysplastic.

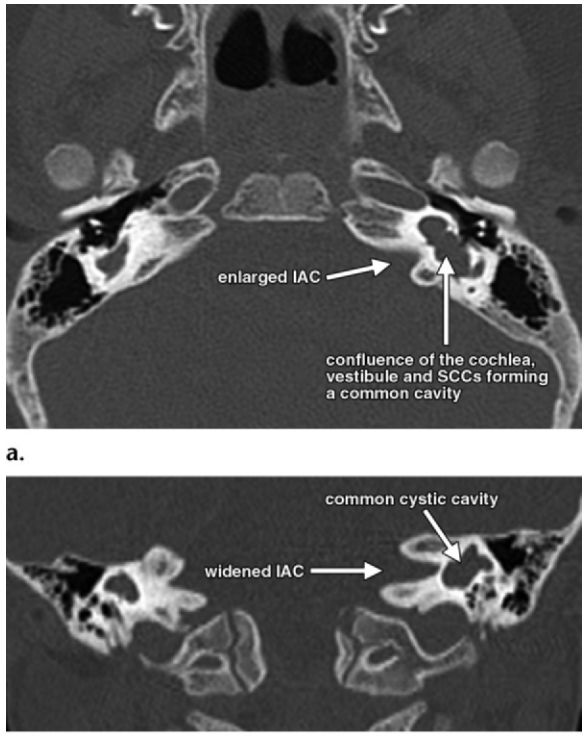

Figure 7. Common cavity malformation in a 2-year-old girl with profound bilateral SNHL and cleft palate. Axial **(a)** and coronal **(b)** CT images show confluence of a globular left cochlea with a globular enlarged left vestibule and dysmorphic left lateral and superior semicircular canals *(SCCs)*. The right cochlea is absent, and there is an enlarged globular right vestibule with absence of the right lateral and posterior semicircular canals.

trisomy 21, Goldenhar, and Crouzon syndromes. The following discussion is not meant to be a comprehensive review of congenital ear malformations; instead, it is a brief overview of some of the more common congenital entities involving the external, middle, and inner ear.

Congenital atresia of the EAC involves a spectrum of abnormalities in which the EAC fails to develop fully. The resultant abnormality may be classified as osseous, membranous, or mixed depending on the degree of development of the EAC. Furthermore, the atresia may be bilateral or, more commonly, unilateral (Fig 5) and is often associated with abnormalities of the pinna. The prevalence of atresia of the EAC is approximately one in 10,000 (3). Imaging of the temporal bone aids in surgical planning by allowing assessment of the size and pneumatization of the middle ear, potential associated abnormalities of the ossicles (4), and the location of the mastoid segment of the facial nerve, which is often displaced anteriorly (5).

Imaging abnormalities involving the bony labyrinth are present in 20%–40% of patients with SNHL (6,7). CT is currently insensitive to abnormalities of the membranous labyrinth, which are responsible for most cases of SNHL. The specific timing of the insult during inner ear development determines the resultant malformation type along a spectrum of congenital inner ear malformations (6), which include labyrinthine (Michel) aplasia, cochlear aplasia (Fig 6), common cavity malformation (Fig 7), incomplete partition type I (cystic cochleovestibular malformation) (Fig 8), incomplete partition type II (classic Mondini malformation) (Fig 9), and cochleovestibular hypoplasia. Historically, all abnormalities of partitioning of the cochlea were referred to as Mondini malformation. More recently, Sennaroglu and Saatci (8) categorized incomplete partition of the cochlea

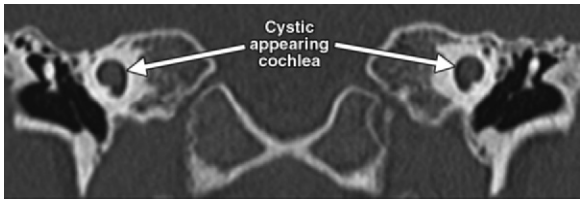

Figure 8. Incomplete partition type I in a 5-year-old girl with profound right SNHL and mild to moderate left SNHL with a conductive component on the left. Coronal CT image shows a cystic-appearing cochlea bilaterally with absence of partitioning.

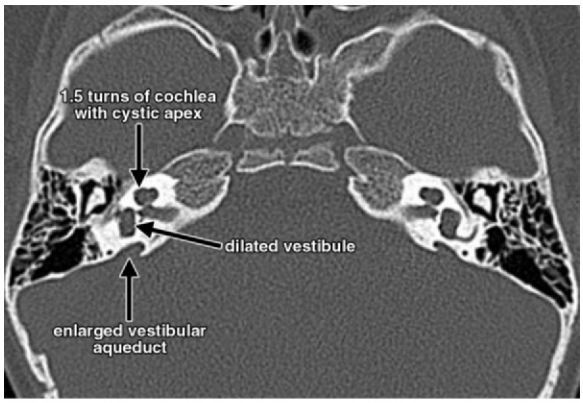

a.

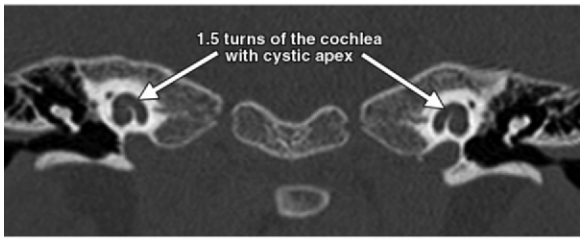

b.

Figure 9. Incomplete partition type II in a 13-month-old boy with bilateral mixed hearing loss. Axial **(a)** and coronal **(b)** CT images show one and one-half turns of the cochlea and cystic dilatation of the apical turn bilaterally. The vestibular aqueducts are enlarged bilaterally.

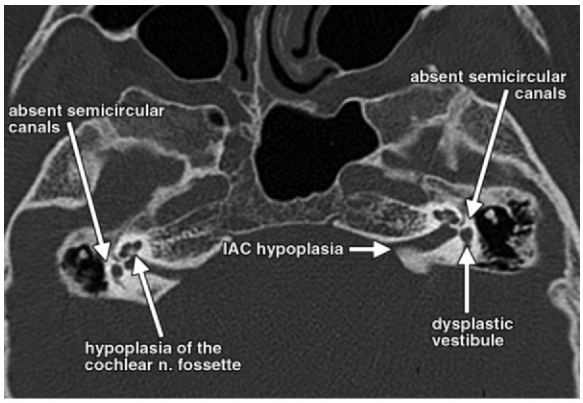

a.

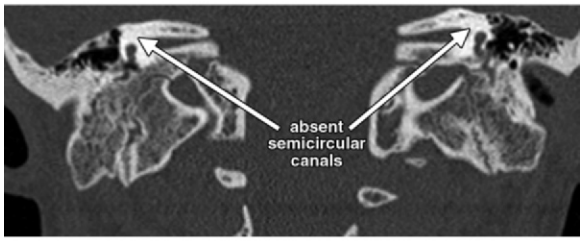

b.

Figure 10. CHARGE syndrome in a 17-year-old boy with bilateral mixed hearing loss. Axial **(a)** and coronal **(b)** CT images show bilateral hypoplastic vestibules and absence of the semicircular canals. The bilateral cochlear nerve fossette and IAC are also hypoplastic. *n.* = nerve.

into two types. In incomplete partition type I, the cochlea completely lacks partitioning and appears as a cystic structure at CT. In incomplete partition type II, the cochlea contains one and one-half turns, with a normal basal turn and a cystic-appearing dilated apical portion. An example of syndromic hearing loss is seen in Figure 10, which shows a patient with CHARGE syndrome.

Enlarged vestibular aqueduct syndrome is a relatively common cause of SNHL. Enlargement of the vestibular aqueduct is the most frequently seen osseous abnormality in patients with SNHL. An enlarged vestibular aqueduct may be seen in isolation (Fig 11) or in association with other abnormalities of the inner ear. A commonly accepted imaging criterion for an enlarged vestibular aqueduct is a caliber of 1.5 mm or greater in the midportion of the aqueduct (9). Enlargement of the vestibular aqueduct may also be suspected if the aqueduct is larger in caliber than the normal lateral semicircular canal.

Vascular abnormalities of the temporal bone may involve the ICA and its branches or the internal jugular vein. Both an aberrant course of the ICA (Fig 12) and a high-riding jugular bulb may manifest as tinnitus. Differentiation of these entities from neoplastic or inflammatory processes with imaging is critical in guiding appropriate clinical management (10).

Persistence of the stapedial artery is rare, with a prevalence of 0.48% (11), but its identification is crucial if middle ear surgery is planned. A persistent stapedial artery may be seen in association with an aberrant ICA (12). At imaging, the persistent stapedial artery can be seen arising from the petrous segment of the ICA or aberrant ICA and extending superiorly to supply the middle meningeal artery. Typical findings include apparent expansion of the tympanic segment of the facial nerve and abnormal soft-tissue attenu-

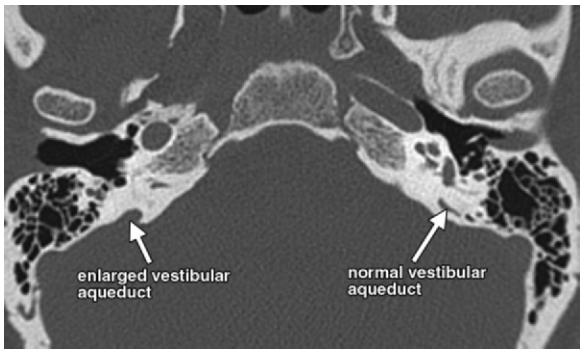

Figure 11. Enlargement of the vestibular aqueduct in a 23-year-old woman. Axial CT image shows an enlarged right vestibular aqueduct. The left vestibular aqueduct is of normal caliber.

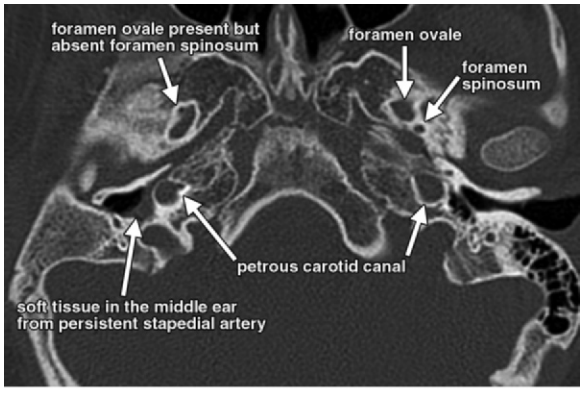

a.

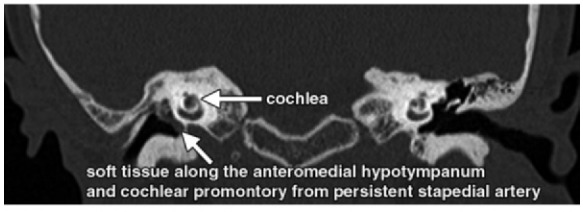

b.

Figure 13. Persistent stapedial artery in an 8-year-old boy with microtia, moderate right conductive hearing loss, and a history of canaloplasty for atresia of the EAC. Axial **(a)** and coronal **(b)** CT images show a persistent stapedial artery arising from the horizontal portion of the carotid artery. Abnormal soft-tissue attenuation lateral to the cochlear promontory and apparent expansion of the tympanic segment of the facial nerve are seen, findings indicative of the aberrant vessel. The foramen spinosum is absent on the right.

ation adjacent to the cochlear promontory (Fig 13) (12,13). In addition, the ipsilateral foramen spinosum is absent (12).

Inflammatory Conditions

Several inflammatory conditions may affect the temporal bone. At imaging, infectious or inflammatory processes can be described according to the degree of involvement of the four anatomic

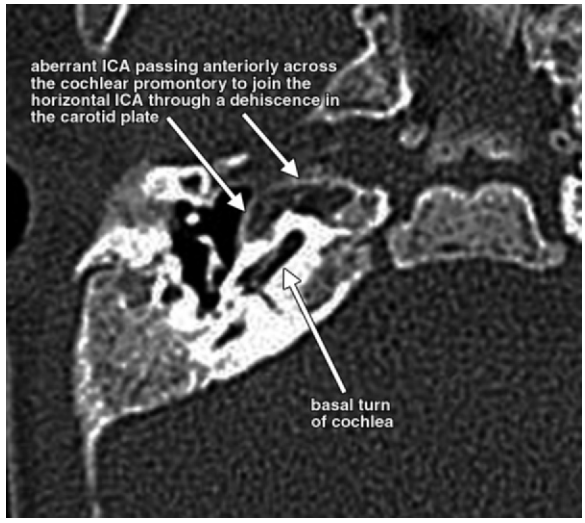

Figure 12. Aberrant ICA. Axial CT image shows an aberrant ICA passing anterior to the cochlear promontory through a dehiscent carotid plate.

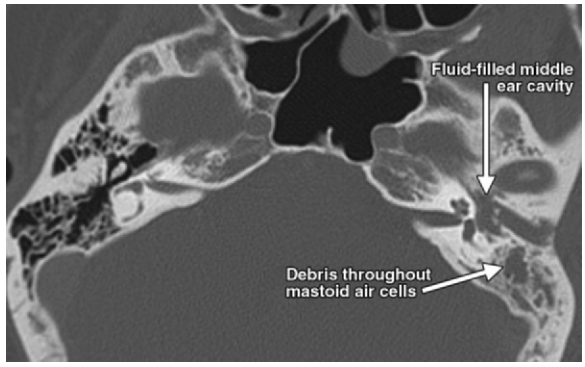

Figure 14. Otitis media in a 28-year-old woman. Axial CT image shows complete opacification of the left middle ear and mastoid air cells by fluid-attenuation material. No erosion of the ossicular chain was present.

regions: external ear, middle ear and mastoid, inner ear, and petrous apex.

Teaching Point

The most common inflammatory condition affecting the temporal bone is acute otitis media (AOM). AOM is the most common disease of childhood for which antibiotics are prescribed in the United States (14). It usually occurs as the sequela of a viral upper respiratory infection with disruption of the mucosal barrier that prevents bacteria in the nose and nasopharynx from spreading to the middle ear. The imaging findings of uncomplicated AOM are nonspecific, with partial or total fluid-attenuation opacification of the middle ear seen at CT (Fig 14). Chronic otomastoiditis typically occurs as a result of long-standing eustachian tube dysfunction (15).

Figure 15. Coalescent mastoiditis in a 49-year-old woman. Axial **(a)** and coronal **(b)** CT images show complete opacification of the mastoid air cells with fluid-attenuation material and loss of internal bone septa. A large defect in the sigmoid sinus plate is present, and there are bone defects in the tegmen mastoideum (white arrowheads in **b**) and the external cortex of the mastoid bone (black arrowheads in **b**).

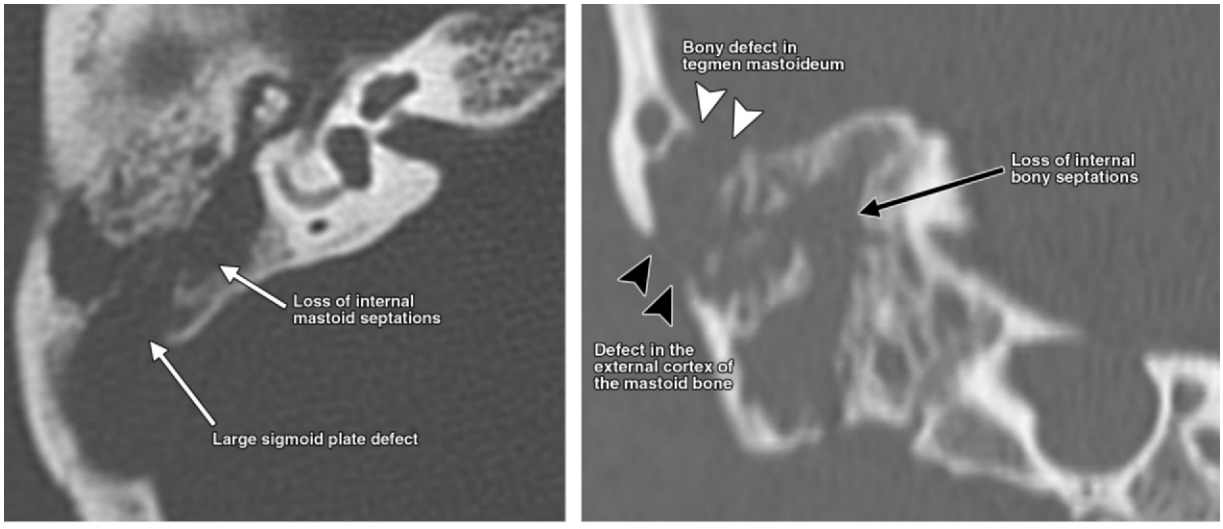

a. **b.**

Figure 16. Dural sinus thrombosis. **(a)** Axial contrast-enhanced CT image shows a filling defect in the left sigmoid sinus. **(b)** Axial nonenhanced two-dimensional time-of-flight MR venographic image shows absent flow in the left jugular bulb and sigmoid sinus.

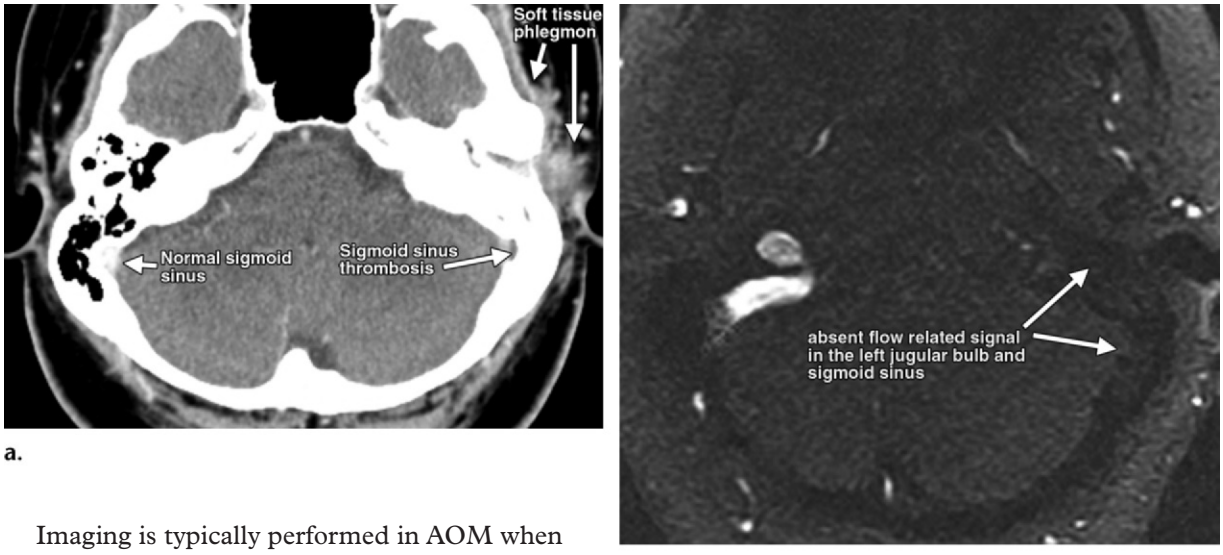

a. **b.**

Imaging is typically performed in AOM when a complication is suspected. Important complications to consider when evaluating acute otomastoiditis include coalescent mastoiditis (Fig 15), Bezold abscess, dural sinus thrombosis (Fig 16), subperiosteal abscess, intracranial abscess and empyema (Fig 17), meningitis, facial nerve involvement, labyrinthitis, and petrous apicitis. These same complications can occasionally occur superimposed on chronic otomastoiditis.

The imaging hallmark of coalescent mastoiditis is the loss of internal bone septa of the mastoid air cells (15) in the setting of fluid or soft-tissue opacification (Fig 15). Bone defects may be seen along the margins of the mastoid air cells (Fig 15). Bezold abscess occurs with erosion of the mastoid tip and adjacent involvement of the posterior digastric muscle insertion; this may ultimately result in mediastinitis as the infection extends inferiorly along the fascial planes (15).

Dural sinus thrombosis may occur by means of erosion of the sigmoid plate (15) or thrombophlebitic spread via emissary veins (16). Common

Figure 17. Epidural abscess in a 23-year-old woman. Axial contrast-enhanced CT **(a)** and coronal contrast-enhanced T1-weighted MR **(b)** images show a rim-enhancing fluid collection in the left temporal epidural space. There is adjacent enhancement of parenchyma and dura.

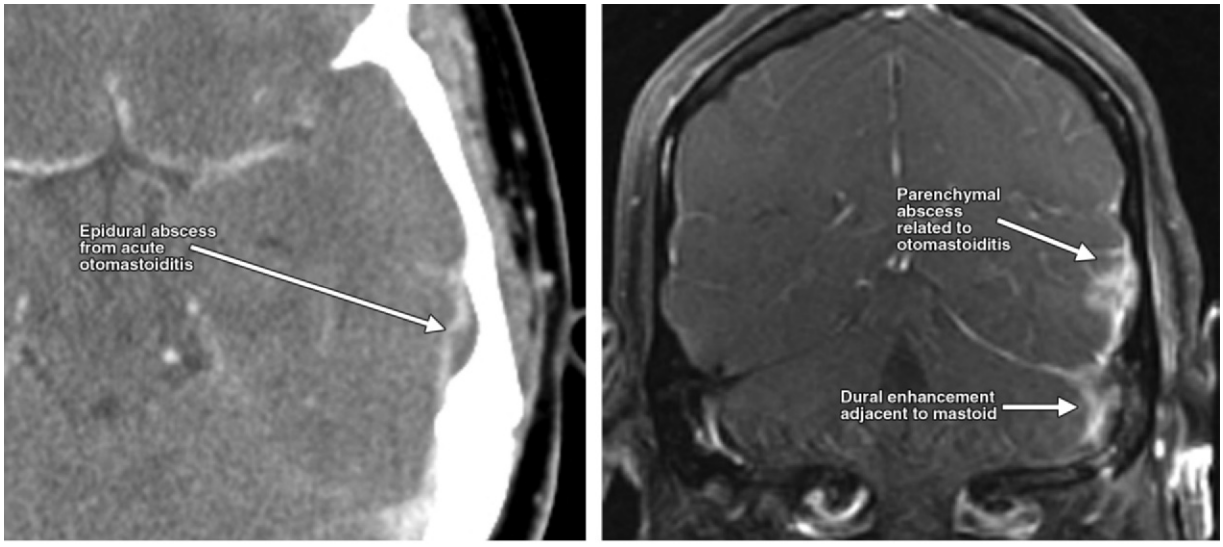

Figure 18. Pars flaccida cholesteatoma in a 63-year-old man. Axial **(a)** and coronal **(b)** CT images show an area of soft-tissue attenuation in the Prussak space with extension into the mastoid antrum, erosion of the incus, and blunting of the scutum.

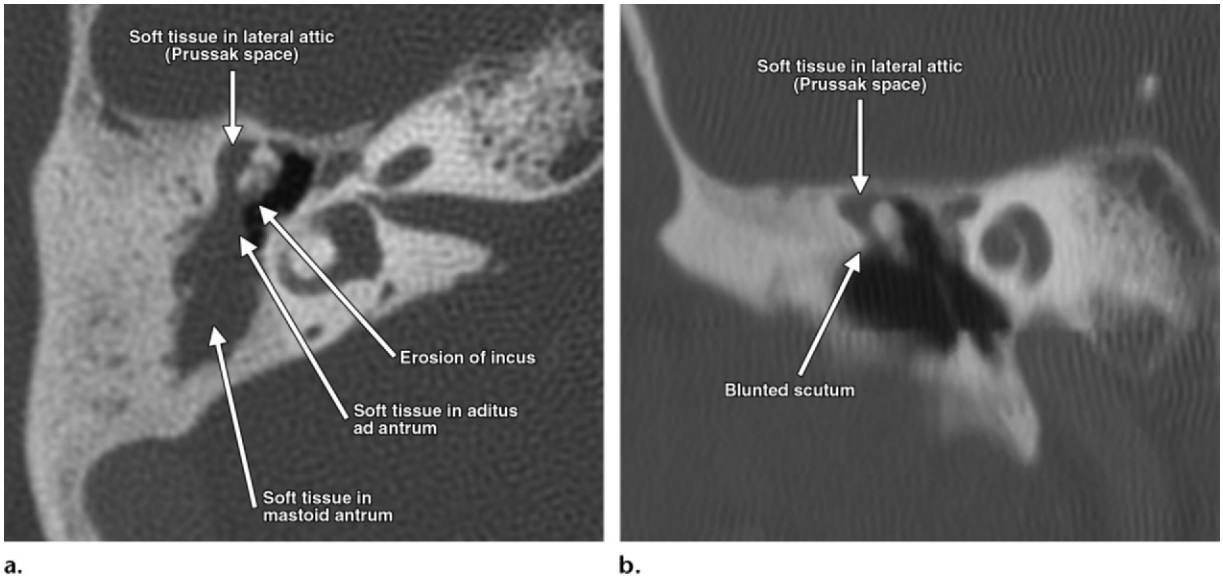

symptoms include headache, otalgia, papilledema, and fever in the setting of AOM (16). Dural sinus thrombosis can be diagnosed with contrast-enhanced CT (17) or two-dimensional time-of-flight or phase-contrast MR venography (18).

Extension of infection beyond the temporal bone, with abscess formation in the subperiosteal, epidural, or intraparenchymal spaces, can be characterized with contrast-enhanced CT or MR imaging. Facial nerve involvement and labyrinthitis are preferentially evaluated with contrast-enhanced MR imaging in the acute setting (19).

Both AOM and chronic otitis media can result in the development of aquired cholesteatomas in the middle ear. A cholesteatoma is a sac lined with ectopic stratified squamous epithelium and filled with exfoliated keratin debris. Most cholesteatomas of the middle ear are acquired (98%); only a minority are congenital.

Acquired cholesteatomas typically arise in the pars flaccida of the tympanic membrane (Fig 18) and less commonly in the pars tensa region. Pars

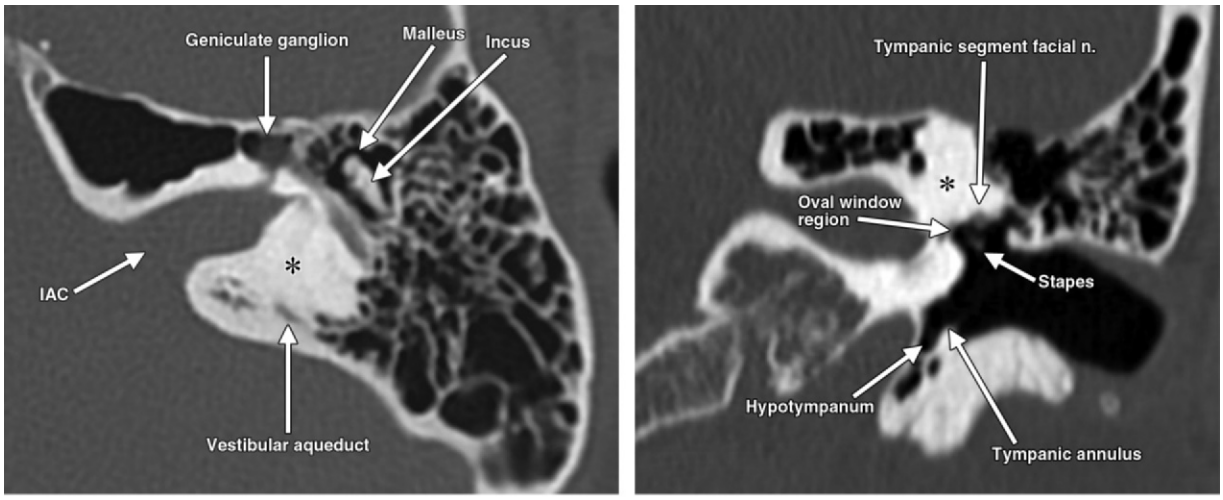

Figure 19. Labyrinthitis ossificans in a 45-year-old woman. **(a, b)** Axial **(a)** and coronal **(b)** CT images show abnormal sclerosis of the bony labyrinth and cochlea (*). *n.* in **b** = nerve. **(c)** Axial T2-weighted MR image shows absence of fluid signal intensity in the left cochlea and semicircular canals.

flaccida cholesteatomas are typically centered in the Prussak space, whereas pars tensa cholesteatomas are typically centered in the sinus tympani or facial recess (15). All types of cholesteatomas may erode the ossicular chain, scutum, mastoid bone, or Körner septum (15,20).

At CT, the soft-tissue attenuation associated with cholesteatoma may be difficult or impossible to differentiate from fluid attenuation in the middle ear associated with chronic otitis media or other inflammatory or infectious conditions (19). However, diffusion-weighted MR imaging may allow differentiation of cholesteatoma from inflammation and infection in the middle ear (21–24).

Labyrinthitis has three radiologic stages: acute, fibrous, and labyrinthitis ossificans. In the acute stage, contrast-enhanced T1-weighted MR imaging may show abnormal enhancement of the labyrinth. MR imaging also allows detection of cochlear obstruction in the fibrous stage, before abnormalities are detectable with CT (25). Labyrinthitis ossificans involves pathologic ossification of the bony labyrinth and cochlea (Fig 19) and is well-depicted with CT (19).

Pneumatization of the petrous apex occurs in 9%–30% of persons (26). When pneumatized, the petrous apex can become involved by middle ear infections. A cholesterol granuloma results from a foreign-body giant cell reaction to the deposition of cholesterol crystals in the air cells with fibrosis and vascular proliferation. The characteristic CT appearance of a cholesterol granuloma is an expansile lesion with smooth margins (Fig 20). MR imaging shows high signal intensity on T1-weighted images and often high signal intensity on T2-weighted images owing to the cholesterol crystals and methemoglobin from repeated hemorrhage (Fig 21) (26).

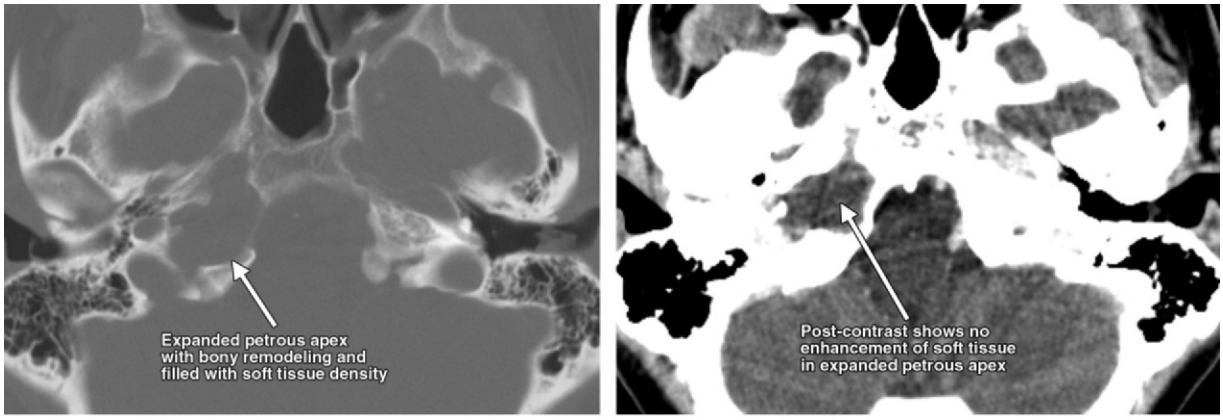

Figure 20. Cholesterol granuloma of the petrous apex in a 52-year-old man. Axial nonenhanced (bone window) **(a)** and contrast-enhanced (brain window) **(b)** CT images show bony expansion of the petrous apex by a nonenhancing mass.

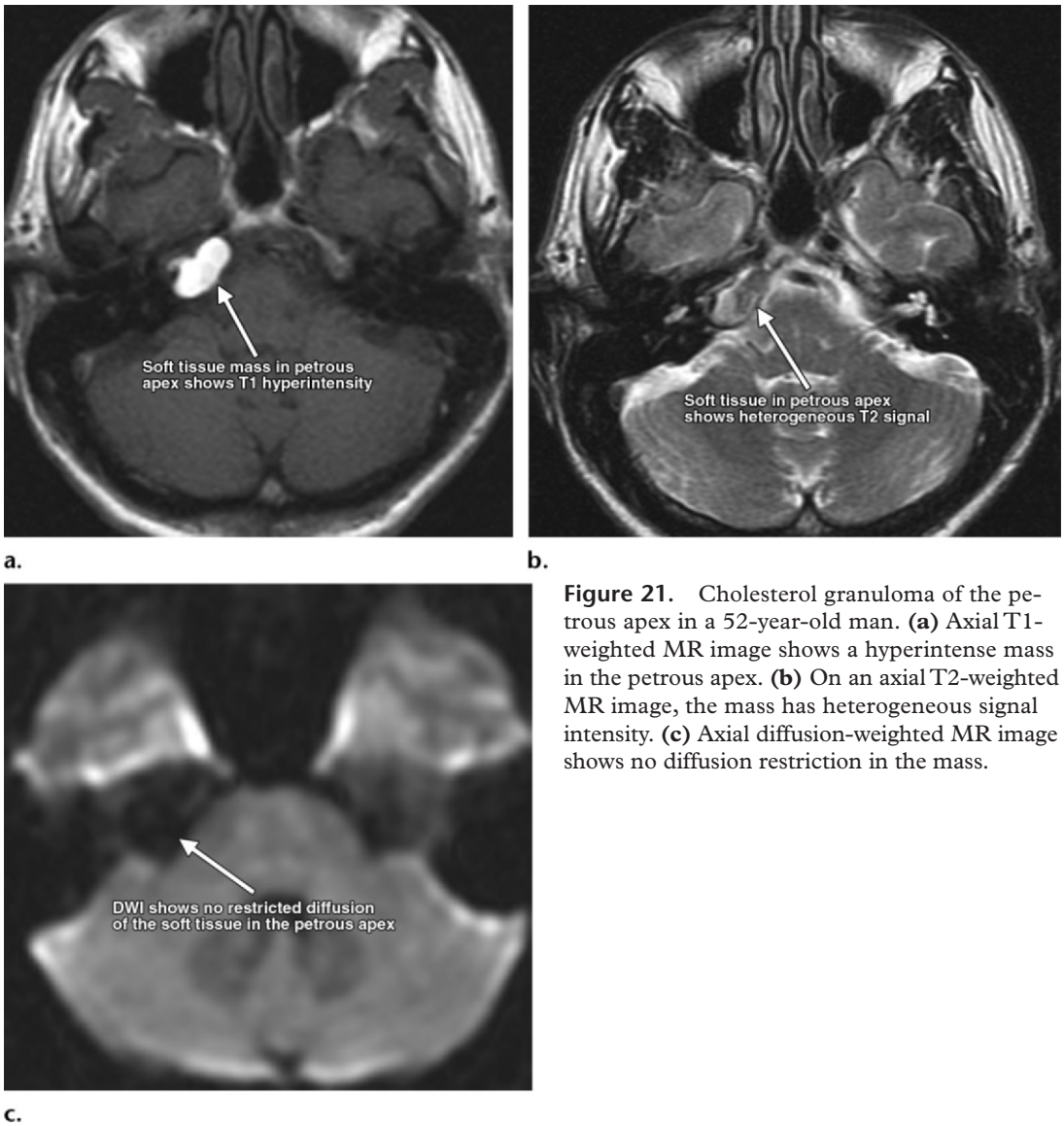

Figure 21. Cholesterol granuloma of the petrous apex in a 52-year-old man. **(a)** Axial T1-weighted MR image shows a hyperintense mass in the petrous apex. **(b)** On an axial T2-weighted MR image, the mass has heterogeneous signal intensity. **(c)** Axial diffusion-weighted MR image shows no diffusion restriction in the mass.

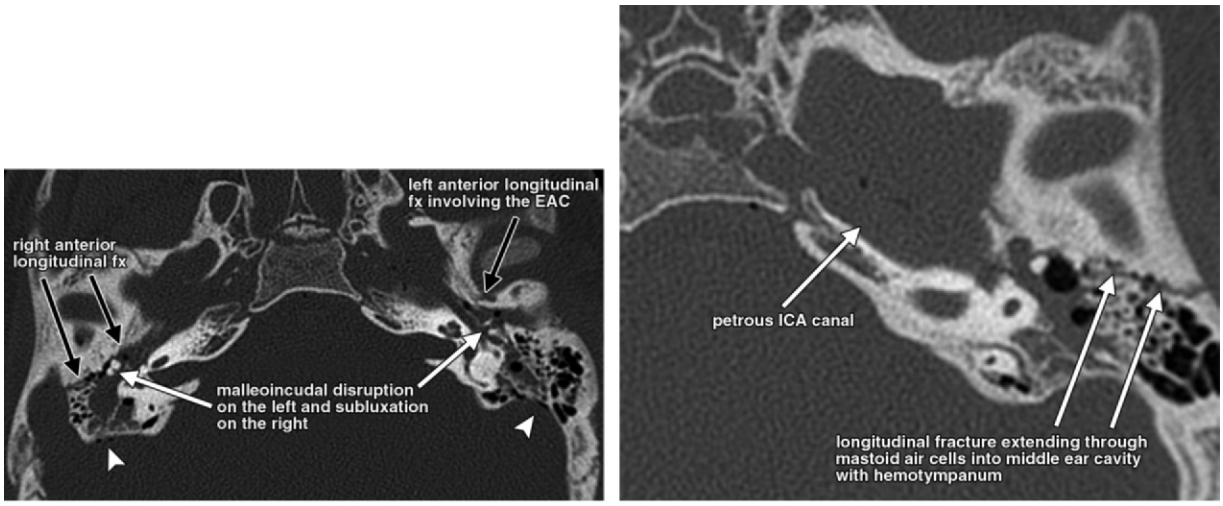

a. b.

Figure 22. Bilateral longitudinal fractures of the temporal bone in a 47-year-old man. Axial CT images show fracture lines (*fx* in **a**) parallel to the long axis of the petrous bone. Bilateral malleoincudal abnormalities (disruption on the left, subluxation on the right) and hemotympanum are noted with fluid attenuation surrounding the ossicles. Air attenuation is faintly seen within the left petrous ICA canal. Arrowheads in **a** = tiny amount of intracranial air.

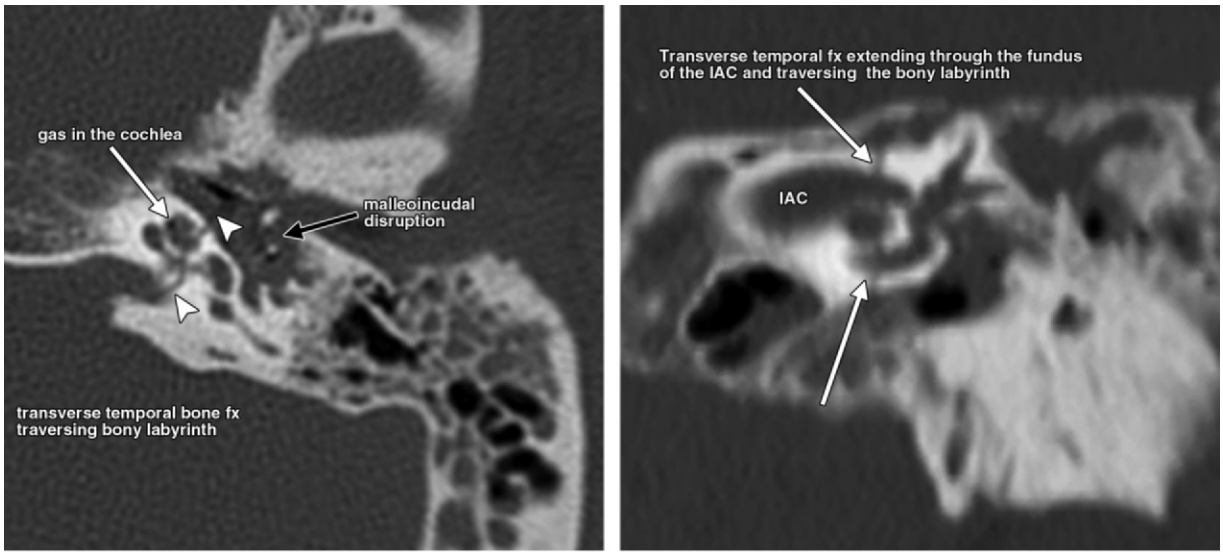

a. b.

Figure 23. Transverse fracture of the left temporal bone with ossicular injury in a 39-year-old man. Axial **(a)** and coronal **(b)** CT images show a fracture line *(fx)* (arrowheads in **a**, arrows in **b**) perpendicular to the long axis of the left petrous bone, traversing the IAC and bony labyrinth. Malleoincudal disruption and hemotympanum are noted. Air attenuation is seen within the cochlea.

Trauma

Historically, temporal bone fractures were classified into two main categories, longitudinal (Fig 22) and transverse (Fig 23), on the basis of the fracture plane relative to the long axis of the petrous bone (27). Additional classification schemes have been proposed that describe temporal bone fractures with respect to involvement of the otic capsule (28) or petrous apex (29). It is now generally recognized that temporal bone fractures may be complex (Fig 24) with mixed features of both longitudinal and transverse fractures.

Teaching Point

The classically described longitudinal fracture runs parallel to the long axis of the petrous bone (Fig 22). Longitudinal fractures typically traverse the middle ear cavity, with frequent disruption

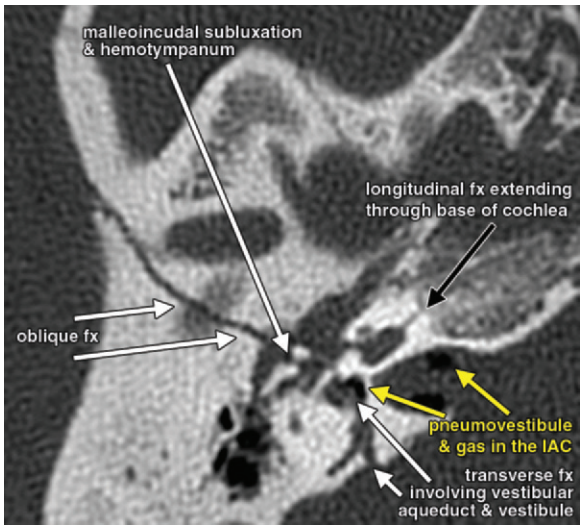

Figure 24. Complex (mixed) fracture of the right temporal bone in a 16-year-old boy. Axial CT image shows oblique, longitudinal, and transverse fracture lines *(fx)*. The oblique fracture traverses the middle ear cavity; there is associated malleoincudal subluxation and hemotympanum. The transverse fracture involves the vestibule and vestibular aqueduct. The longitudinal fracture extends through the base of the cochlea. There is pneumovestibule and gas in the IAC.

of the ossicles and resultant conductive hearing loss (30). The fracture plane is usually extralabyrinthine and anterior to the labyrinthine structures, toward the eustachian tube and middle cranial fossa (30). Less commonly, longitudinal fractures are located posterior to the labyrinth, toward the jugular foramen and posterior cranial fossa. Additional involvement of the EAC, tegmen tympani, and squamosal temporal bone is common. Both subtypes of longitudinal fractures frequently involve the first genu or anterior tympanic segment of the facial nerve. Involvement of the mastoid segment of the facial nerve can be seen with the posterior subtype (30). A rare complication that can occur with the anterior subtype is an epidural hematoma in the middle cranial fossa as a result of vascular injury to the middle meningeal artery (30).

The classically described transverse fracture runs perpendicular to the long axis of the petrous bone (Fig 23). The fracture plane typically extends from the jugular foramen and foramen magnum to the middle cranial fossa, commonly passing through or near the vestibular aqueduct with variable involvement of the otic capsule. There are two subtypes of transverse fractures: medial and lateral relative to the arcuate eminence. Both subtypes frequently result in SNHL.

The medial subtype traverses the fundus of the IAC. SNHL in the setting of a medial transverse fracture may be complete due to transection of the cochlear nerve (30). The lateral subtype traverses the bony labyrinth and may thus result in SNHL. The lateral subtype may also have an associated perilymphatic fistula due to injury of the stapes footplate (30).

Teaching Point

A common complication associated with temporal bone fractures is hearing loss, which may be sensorineural, conductive, or mixed. Conductive hearing loss associated with a temporal bone fracture can be caused by hemotympanum, disruption of the tympanic membrane, or disruption of the ossicular chain (30). Of the ossicles, the incus is the most vulnerable to injury, owing to the anatomy and the supportive ligamentous structures stabilizing the malleus and stapes. As a result, most ossicular dislocations or subluxations involve the incus (30). The most common injuries are incudostapedial joint subluxation, malleoincudal subluxation, incus dislocation, and dislocation of the malleoincudal complex. Less common ossicular injuries include stapedial and mallear fractures (27).

Other complications related to temporal bone fractures include facial nerve injury, perilymphatic fistula, vertigo, cerebrospinal fluid leak, meningitis, and acquired cholesteatoma.

Tumors and Tumorlike Conditions

Many types of tumors may affect the temporal bone. A temporal bone tumor may be clinically suspected in several clinical scenarios. Four common clinical presentations suspicious for a tumor are *(a)* SNHL, tinnitus, or vertigo, which may indicate a vestibular schwannoma or other cerebellopontine angle mass; *(b)* pulsatile tinnitus or cranial neuropathy involving the jugular foramen; *(c)* peripheral facial nerve dysfunction (31); and *(d)* a previously clinically identified tumor of the temporal bone. There are also nonneoplastic conditions, including various otodystrophies, that can mimic a neoplasm at imaging.

The most common tumor to affect the temporal bone at the cerebellopontine angle is the vestibular schwannoma (Fig 25) (32). Less commonly, schwannomas can be isolated to the facial nerve (Fig 26) (33). A schwannoma is a benign, slow-growing neoplasm (32) that arises from the nerve sheath and is composed of Schwann cells in a collagenous matrix. Vestibular schwannomas can

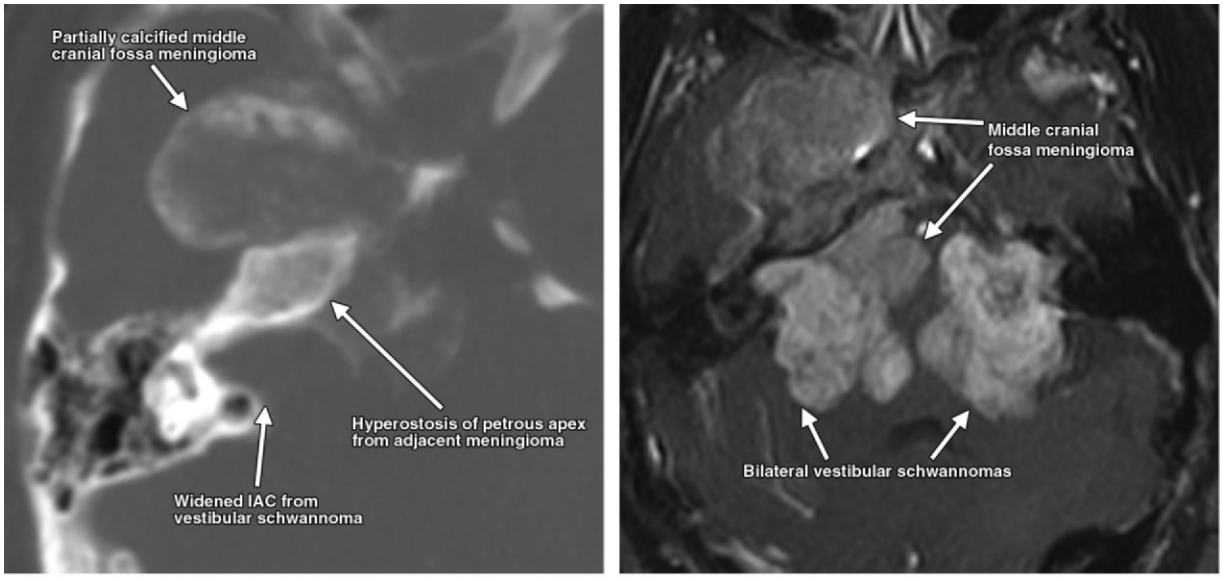

Figure 25. IAC schwannoma and meningioma in a 24-year-old man with neurofibromatosis type 2. **(a)** Axial CT image shows a partially calcified meningioma in the middle cranial fossa with adjacent hyperostosis of the petrous apex. The ipsilateral IAC is widened from the patient's known vestibular schwannoma. **(b)** Axial gadolinium-enhanced T1-weighted MR image shows varying degrees of relatively homogeneous enhancement of the meningioma and bilateral vestibular schwannomas.

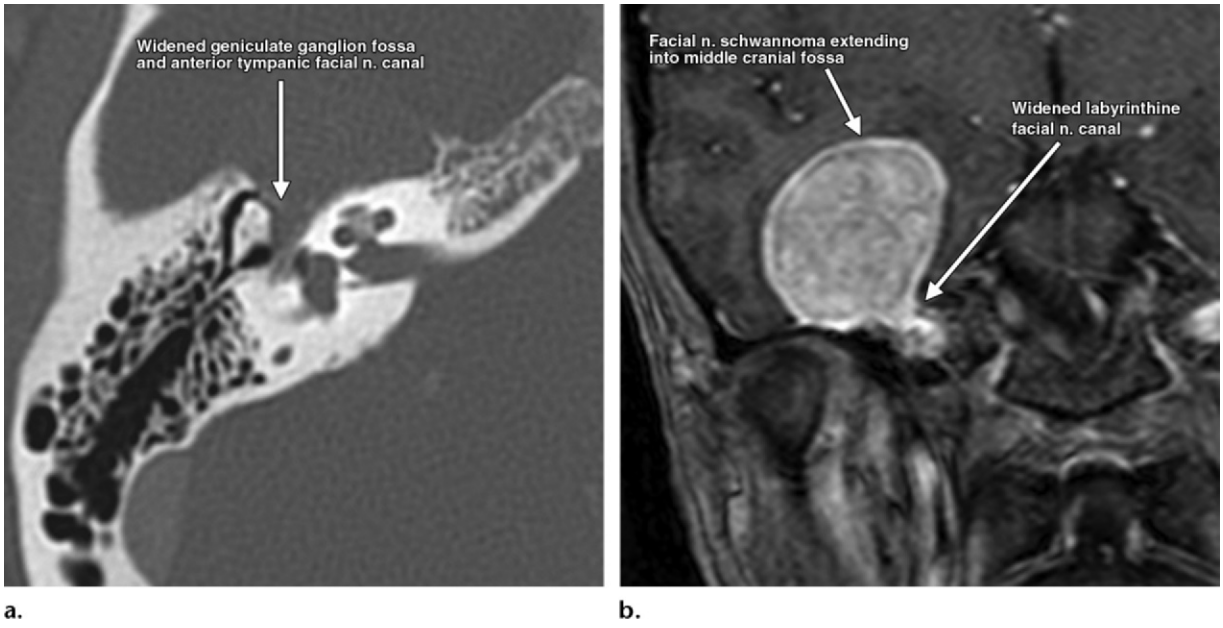

Figure 26. Facial nerve schwannoma. **(a)** Axial CT image shows a mass centered in the geniculate ganglion with widening of the geniculate fossa and anterior portion of the tympanic segment of the facial nerve *(n.)* canal. **(b)** Coronal gadolinium-enhanced T1-weighted MR image shows homogeneous enhancement of the mass, which extends into the middle cranial fossa. The labyrinthine segment of the facial nerve *(n.)* canal also appears widened.

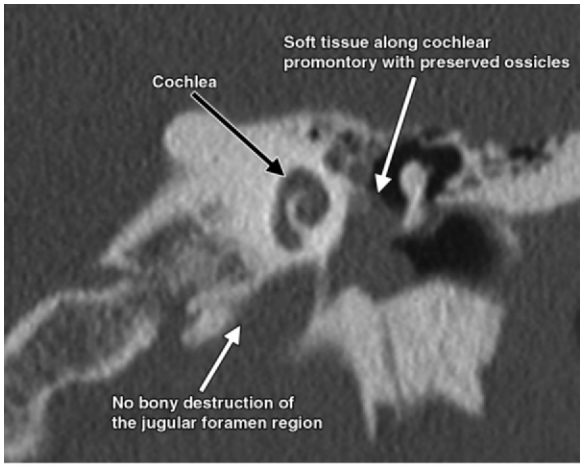

a.

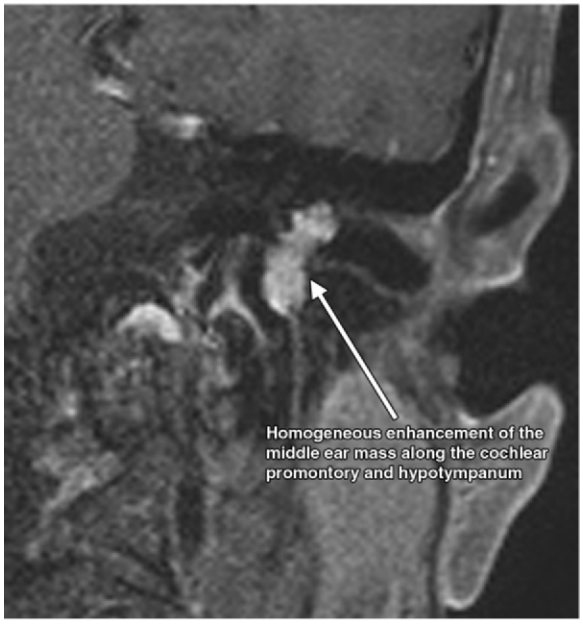

b.

Figure 27. Glomus tympanicum tumor in a 54-year-old man. **(a)** Coronal CT image shows a soft-tissue mass along the cochlear promontory and hypotympanum with preservation of the ossicular chain. **(b)** Coronal gadolinium-enhanced T1-weighted MR image shows that the mass has homogeneous enhancement.

occur in isolation or in association with neurofibromatosis type 2 (Fig 25), which should be suspected in cases of bilateral vestibular schwannomas (34,35). Typical MR imaging findings of acoustic schwannoma are a mass centered in the porus acusticus that is isointense or hypointense to gray matter on T1-weighted images and slightly hyperintense to gray matter on T2-weighted images (34). Lesions typically show homogeneous enhancement on contrast-enhanced T1-weighted images (34).

A tumor that less commonly occurs in the cerebellopontine angle and involves the temporal

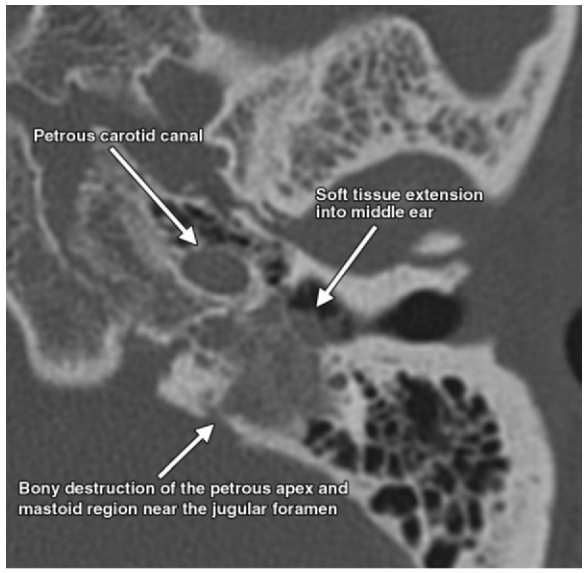

a.

b.

Figure 28. Glomus jugulare tumor in a 36-year-old man. **(a)** Axial CT image shows bone destruction from a mass in the posterior petrous apex and mastoid region near the jugular foramen. There is soft-tissue extension into the middle ear. **(b)** Axial gadolinium-enhanced T1-weighted MR image shows avid enhancement of the mass.

bone is the meningioma (34). This tumor is also seen in association with neurofibromatosis type 2 (Fig 25). Isolated meningiomas can occur elsewhere in the cranium, including more commonly the olfactory groove, sphenoid wing, planum sphenoidale, and supratentorially.

Teaching Point

Paragangliomas, also known as glomus tumors or chemodectomas, are the second most common tumor to involve the temporal bone (36) and the most common tumor of the middle ear. These tumors originate from paraganglia along the tympanic branch of the glossopharyngeal nerve (Jacobson nerve) and the auricular branch of the vagus nerve (Arnold nerve) and within the intravagal paraganglia inferior to the foramen (Figs 27, 28). Paragangliomas are highly vascular.

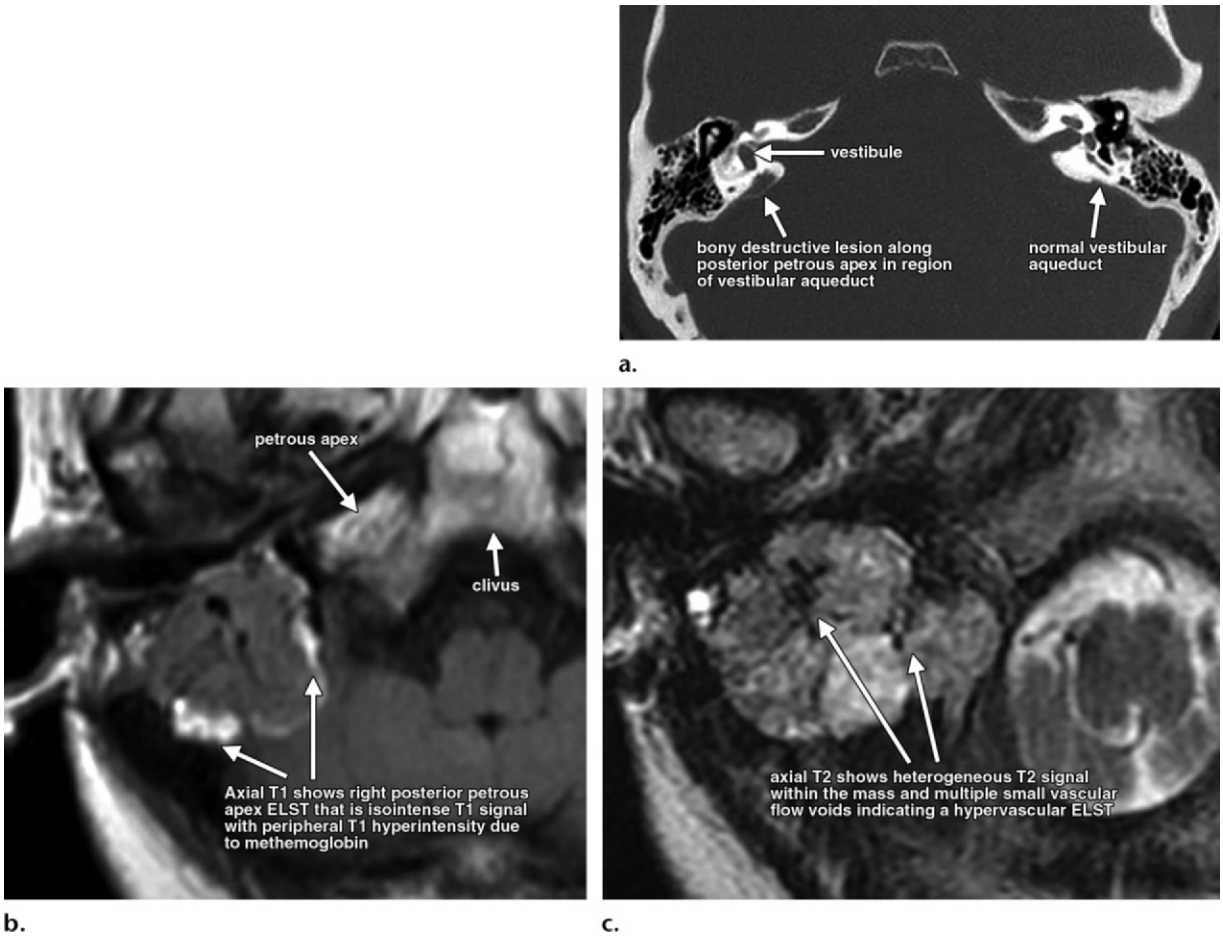

Figure 29. ELST in two patients. **(a)** Axial CT image shows bone destruction along the right posterior petrous apex in the region of the vestibular aqueduct. **(b)** Axial T1-weighted MR image in another patient, a 60-year-old woman, shows a mass in the posterior petrous apex. The mass is isointense to adjacent brain tissue with peripheral high signal intensity from methemoglobin. **(c)** Axial T2-weighted MR image in the same patient as in **b** shows that the mass has heterogeneous signal intensity with multiple small flow voids (arrows).

Glomus jugulare tumor can result in bone destruction as the tumor grows (37). Paragangliomas may have a typical salt-and-pepper appearance on T1-weighted and T2-weighed images due to intermixed vascular flow voids and tumor tissue (37). They usually show avid enhancement on gadolinium-enhanced images (37).

Endolymphatic sac tumors (ELSTs) occur along the posterior petrous apex and typically involve the vestibular aqueduct. These tumors are locally invasive papillary cystadenomatous tumors arising from the endolymphatic sac. ELSTs usually occur sporadically. Less commonly, ELSTs arise in patients with von Hippel–Lindau disease (31). The tumors cause local bone destruction as they grow. ELSTs are hypervascular tumors, with intratumoral hemorrhage commonly seen at MR imaging (Fig 29). Central calcification and posterior rim calcification are frequently seen at CT (31).

Otospongiosis, also known as otosclerosis, is an unusual disease that affects the otic capsule, resulting in progressive hearing loss. The disease typically affects women more than men, with a female-to-male ratio of 2:1 (38). In otospongiosis, the normal endochondral bone of the otic

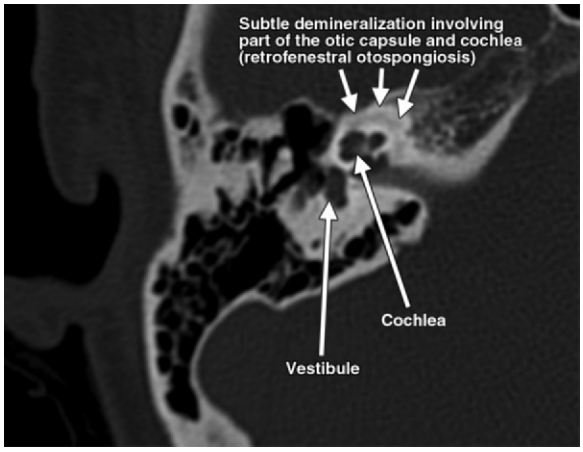

Figure 30. Early otospongiosis. Axial CT image shows subtle demineralization involving part of the otic capsule and cochlea from early retrofenestral otospongiosis.

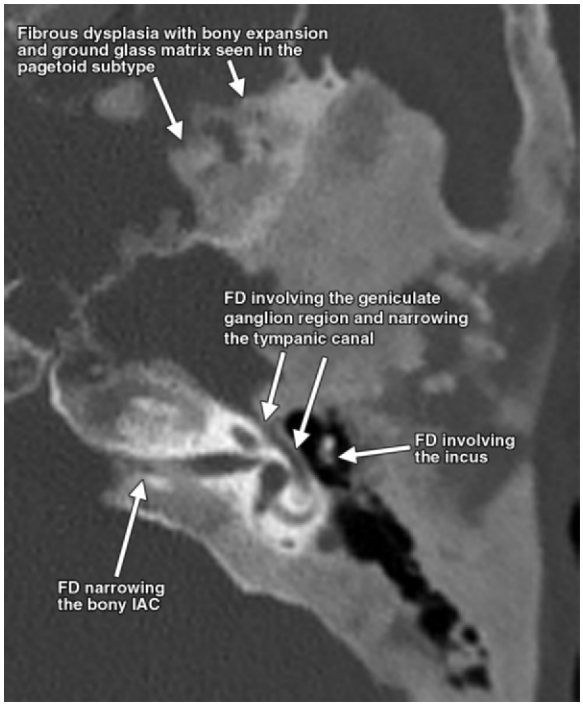

Figure 31. Fibrous dysplasia in a 23-year-old woman. Axial CT image shows expansion of the temporal bone with a ground-glass matrix, as seen in the pagetoid subtype of fibrous dysplasia *(FD)*. There is narrowing of the IAC and the tympanic segment of the facial nerve canal. Involvement of the incus is noted.

capsule is replaced by spongy vascular irregular bone (Fig 30) (38). There are two categories of otospongiosis: fenestral and retrofenestral. The more common fenestral type affects the lateral wall of the bony labryinth, including the oval and round windows, promontory, and facial nerve canal. The less common retrofenestral type primarily involves the otic capsule but usually has fenestral involvement (38).

Fibrous dysplasia is an inherited disorder affecting the bones and can be monostotic or polyostotic. The disease is characterized by inability to form mature lamellar bone owing to disordered osteoblastic activity. As a result, there is gradual replacement of normal bone by an abnormal proliferation of isomorphic fibrous tissue elements intermixed with irregular trabeculae of woven bone (38). This results in bone expansion, which can cause osseous narrowing of the vascular channels and neuroforamina (38) and structurally weakened bone (Fig 31). There are three types of fibrous dysplasia, with variable appearances depending on the proportions of fibrous tissue and osseous elements: pagetoid, sclerotic, and cystic (38).

There are also two bone tumors, aneurysmal bone cyst (Fig 32) and osteochondroma (Fig 33), that uncommonly arise from the temporal bone. These tumors have imaging features similar to those of their counterparts elsewhere in the skeleton (39).

a. b.

Figure 32. Aneurysmal bone cyst. **(a)** Axial CT image shows an expansile bone lesion arising from the inner table of the squamosal temporal bone with internal osseous septa. **(b)** On an axial T2-weighted MR image, the lesion has mixed signal intensity with fluid-fluid levels.

Figure 33. Osteochondroma in a 53-year-old woman. Axial CT image shows a pedunculated osteochondroma (arrow) arising from the petrous apex with apparent narrowing of the adjacent IAC.

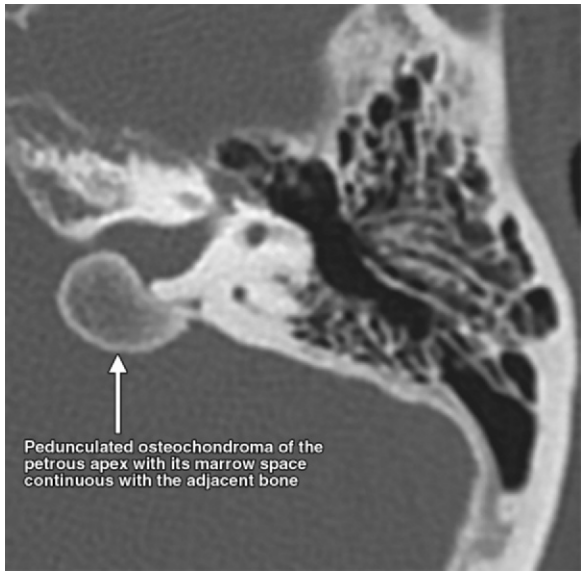

Conclusions

The images of normal temporal bone anatomy in this article and in the supplemental interactive atlas (*http://uwmsk.org/temporalbone/index.html*) facilitate recognition of the imaging features of a spectrum of pathologic conditions of the temporal bone. The interactive atlas also includes a self-assessment quiz. These materials may help residents, neuroradiology fellows, and practicing radiologists achieve mastery of the normal anatomy and pathologic conditions of the temporal bone.

References

1. Swartz JD, Harnsberger HR. Imaging of the temporal bone. 3rd ed. New York, NY: Thieme, 1998.
2. Ozgen B, Cunnane ME, Caruso PA, Curtin HD. Comparison of 45 degrees oblique reformats with axial reformats in CT evaluation of the vestibular aqueduct. AJNR Am J Neuroradiol 2008;29(1):30–34.
3. Mayer TE, Brueckmann H, Siegert R, Witt A, Weerda H. High-resolution CT of the temporal bone in dysplasia of the auricle and external auditory canal. AJNR Am J Neuroradiol 1997;18(1):53–65.
4. Yuen HY, Ahuja AT, Wong KT, Yue V, van Hasselt AC. Computed tomography of common congenital lesions of the temporal bone. Clin Radiol 2003;58(9):687–693.
5. Swartz JD, Faerber EN. Congenital malformations of the external and middle ear: high-resolution CT findings of surgical import. AJR Am J Roentgenol 1985;144(3):501–506.

6. Jackler RK, Luxford WM, House WF. Congenital malformations of the inner ear: a classification based on embryogenesis. Laryngoscope 1987;97(3 pt 2, suppl 40):2–14.
7. Purcell D, Johnson J, Fischbein N, Lalwani AK. Establishment of normative cochlear and vestibular measurements to aid in the diagnosis of inner ear malformations. Otolaryngol Head Neck Surg 2003; 128(1):78–87.
8. Sennaroglu L, Saatci I. A new classification for cochleovestibular malformations. Laryngoscope 2002; 112(12):2230–2241.
9. Rodriguez K, Shah RK, Kenna M. Anomalies of the middle and inner ear. Otolaryngol Clin North Am 2007;40(1):81–96.
10. Fatterpekar GM, Doshi AH, Dugar M, Delman BN, Naidich TP, Som PM. Role of 3D CT in the evaluation of the temporal bone. RadioGraphics 2006;26 (spec issue):S117–S132.
11. Moreano EH, Paparella MM, Zelterman D, Goycoolea MV. Prevalence of facial canal dehiscence and of persistent stapedial artery in the human middle ear: a report of 1000 temporal bones. Laryngoscope 1994;104(3 pt 1):309–320.
12. Silbergleit R, Quint DJ, Mehta BA, Patel SC, Metes JJ, Noujaim SE. The persistent stapedial artery. AJNR Am J Neuroradiol 2000;21(3):572–577.
13. Thiers FA, Sakai O, Poe DS, Curtin HD. Persistent stapedial artery: CT findings. AJNR Am J Neuroradiol 2000;21(8):1551–1554.
14. Gould JM, Matz PS. Otitis media. Pediatr Rev 2010;31(3):102–116.
15. Maroldi R, Farina D, Palvarini L, et al. Computed tomography and magnetic resonance imaging of pathologic conditions of the middle ear. Eur J Radiol 2001;40(2):78–93.
16. Viswanatha B, Naseeruddin K. Lateral sinus thrombosis in otology: a review. Mediterr J Hematol Infect Dis 2010;2(3):e2010027.
17. Goldberg AL, Rosenbaum AE, Wang H, Kim WS, Lewis VL, Hanley DF. Computed tomography of dural sinus thrombosis. J Comput Assist Tomogr 1986;10(1):16–20.
18. Davison SP, Facer GW, McGough PF, McCaffrey TV, Reder PA. Use of magnetic resonance imaging and magnetic resonance angiography in diagnosis of sigmoid sinus thrombosis. Ear Nose Throat J 1997;76(7):436–441.
19. Lemmerling MM, De Foer B, Verbist BM, VandeVyver V. Imaging of inflammatory and infectious diseases in the temporal bone. Neuroimaging Clin N Am 2009;19(3):321–337.
20. Swartz JD. Imaging of the temporal bone. New York, NY: Thieme, 1986.
21. Aikele P, Kittner T, Offergeld C, Kaftan H, Hüttenbrink KB, Laniado M. Diffusion-weighted MR imaging of cholesteatoma in pediatric and adult patients who have undergone middle ear surgery. AJR Am J Roentgenol 2003;181(1):261–265.
22. De Foer B, Vercruysse JP, Bernaerts A, et al. Detection of postoperative residual cholesteatoma with non-echo-planar diffusion-weighted magnetic resonance imaging. Otol Neurotol 2008;29(4):513–517.
23. De Foer B, Vercruysse JP, Bernaerts A, et al. The value of single-shot turbo spin-echo diffusion-weighted MR imaging in the detection of middle ear cholesteatoma. Neuroradiology 2007;49(10): 841–848.
24. De Foer B, Vercruysse JP, Pilet B, et al. Single-shot, turbo spin-echo, diffusion-weighted imaging versus spin-echo-planar, diffusion-weighted imaging in the detection of acquired middle ear cholesteatoma. AJNR Am J Neuroradiol 2006;27(7):1480–1482.
25. Isaacson B, Booth T, Kutz JW Jr, Lee KH, Roland PS. Labyrinthitis ossificans: how accurate is MRI in predicting cochlear obstruction? Otolaryngol Head Neck Surg 2009;140(5):692–696.
26. Isaacson B, Kutz JW, Roland PS. Lesions of the petrous apex: diagnosis and management. Otolaryngol Clin North Am 2007;40(3):479–519.
27. Saraiya PV, Aygun N. Temporal bone fractures. Emerg Radiol 2009;16(4):255–265.
28. Brodie HA, Thompson TC. Management of complications from 820 temporal bone fractures. Am J Otol 1997;18(2):188–197.
29. Ishman SL, Friedland DR. Temporal bone fractures: traditional classification and clinical relevance. Laryngoscope 2004;114(10):1734–1741.
30. Swartz JD. Temporal bone trauma. Semin Ultrasound CT MR 2001;22(3):219–228.
31. Patel NP, Wiggins RH 3rd, Shelton C. The radiologic diagnosis of endolymphatic sac tumors. Laryngoscope 2006;116(1):40–46.
32. Swartz JD. Lesions of the cerebellopontine angle and internal auditory canal: diagnosis and differential diagnosis. Semin Ultrasound CT MR 2004;25 (4):332–352.
33. Veillon F, Taboada LR, Eid MA, et al. Pathology of the facial nerve. Neuroimaging Clin N Am 2008;18 (2):309–320.
34. Spickler EM, Govila L. The vestibulocochlear nerve. Semin Ultrasound CT MR 2002;23(3):218–237.
35. Ho SY, Kveton JF. Acoustic neuroma: assessment and management. Otolaryngol Clin North Am 2002;35(2):393–404.
36. Jackson CG. Glomus tympanicum and glomus jugulare tumors. Otolaryngol Clin North Am 2001;34 (5):941–970.
37. Noujaim SE, Pattekar MA, Cacciarelli A, Sanders WP, Wang AM. Paraganglioma of the temporal bone: role of magnetic resonance imaging versus computed tomography. Top Magn Reson Imaging 2000;11(2):108–122.
38. Swartz JD. The otodystrophies: diagnosis and differential diagnosis. Semin Ultrasound CT MR 2004; 25(4):305–318.
39. Shah GV, Doctor MR, Shah PS. Aneurysmal bone cyst of the temporal bone: MR findings. AJNR Am J Neuroradiol 1995;16(4):763–766.

RadioGraphics

Interactive Web-based Learning Module on CT of the Temporal Bone: Anatomy and Pathology

Grace S. Phillips, MD • Sung E. LoGerfo, MD • Michael L. Richardson, MD •Yoshimi Anzai, MD

RadioGraphics 2012; 32:E85–E105 • **Published online** 10.1148/rg.323115117 • **Content Codes:** CT HN NR

Page E90
Developmental malformations that affect the EAC and middle ear may cause conductive hearing loss, whereas those that affect the membranous and bony labyrinth may result in sensorineural hearing loss (SNHL).

Page E93
The most common inflammatory condition affecting the temporal bone is acute otitis media (AOM).

Page E98 (Figure on page E99)
It is now generally recognized that temporal bone fractures may be complex (Fig 24) with mixed features of both longitudinal and transverse fractures.

Page E99
A common complication associated with temporal bone fractures is hearing loss, which may be sensorineural, conductive, or mixed.

Page E101
Paragangliomas, also known as glomus tumors or chemodectomas, are the second most common tumor to involve the temporal bone (36) and the most common tumor of the middle ear.